BISTATIC RADAR OBSERVATIONS OF THE MOON USING THE ARECIBO OBSERVATORY & MINI-RF ON LRO. D. B. J. Bussey[1], G. W. Patterson[1], F. S. Turner[1], R. Schulze[1], D. E. Wahl[2], I. Erteza[2], M. Nolan[3], J. R. Jensen[1], D. A. Yocky[2], A. M. Stickle[1], L. Carter[4], C. V. Jakowatz[2], P. D. Spudis[4] and the Mini-RF Team, [1]Applied Physics Laboratory, Laurel MD, [2]Sandia National Laboratory, Albuquerque NM, [3]Arecibo Observatory, Arecibo PR, [4]Lunar and Planetary Institute, Houston TX..

Introduction: The Mini-RF team has been acquiring bistatic radar measurements of the lunar surface to understand the scattering properties of materials as a function of bistatic angle. These observations have produced the first lunar radar images ever collected with non-zero bistatic angles. The goal of these observations is to test the hypothesis that some permanently shadowed areas near the lunar poles contain water ice.

Rationale: The bistatic angle is determined by the positions and orientations of the radar transmitter and receiver. For radar observations that use the same antenna to transmit and receive a signal, the bistatic angle is zero, and they are referred to as monostatic.

NASA's Mini-RF instrument on the Lunar Reconnaissance Orbiter is currently operating in a bistatic mode with the Arecibo Observatory acting as the transmitter and the Mini-RF antenna acting as the receiver. In this mode, Arecibo transmits a circular polarized S-band signal that is reflected off the lunar surface and into the Mini-RF antenna. Mini-RF receives orthogonal linear polarizations as well as their relative phase (equivalent to the hybrid dual-polarimetric architecture of the monostatic mode [1]) allowing for the calculation of the Stokes parameters (S_1, S_2, S_3, S_4) that characterize the backscattered signal (and the daughter products derived from those parameters).

The circular polarization ratio,

$$CPR = (S_1 - S_4)/(S_1 + S_4)$$

is a product of the Stokes parameters that is often utilized in analyses of planetary radar data [2-5]. This ratio provides an indication of surface roughness, as determined by the distribution of surface and buried wavelength-scale scatterers (*e.g.*, boulders). Typical dry lunar surface has a CPR value less than unity [3]. Higher CPR signals can result from multiple-bounce backscatter off rocky surfaces or from the combined volume scattering and coherent backscatter opposition effects (CBOE) of an ice/regolith mixture [3]. High CPR caused by a rocky surface should be relatively insensitive to the bistatic angle, whilst high CPR caused by ice should be very sensitive to the bistatic angle. I.e., CPR values should decrease abruptly for ice/regolith mixtures at bistatic angles greater than about 1-2° (figure 1).

Monostatic radar data of the lunar surface clearly show that craters and their ejecta typically have elevated CPR values, with respect to background lunar terrain [6]. This is especially characteristic of young, fresh craters and indicates that the crater and its ejecta have a higher fraction of cm- to m-scale scatterers at the surface and/or buried to depths that scale with the wavelength of the transmitted radar signal.

Recent work using Mini-RF on LRO and Mini-SAR data from India's lunar Chandrayaan-1 spacecraft [7] (2008-9), has shown that some permanently shadowed 'anomolous' craters near both poles show elevated CPR interior to the crater rim but low CPR exterior to the crater rim [3,4]. This has been interpreted as consistent with RF backscatter caused by crater interior deposits of an ice/regolith mixture. However, as CPR is a non-unique descriptor of physical composition, we cannot be certain with existing data alone that the anomalous scattering is caused by the presence of ice.

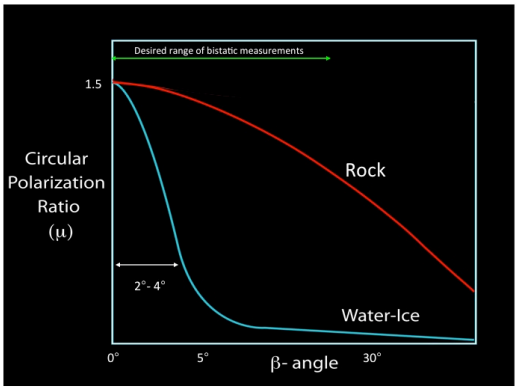

Figure 1. Predicted behavior of CPR versus beta angle for both rocky terrains and an ice/regolith mixture. We are now collecting data that allows ud to actually plot these lines for different terrains.

Observations: To further investigate the nature of the RF signature associated with anomalous craters, we are imaging non-polar and polar targets that have high monostatic CPR values for a range of bistatic angles (figure 2). Non-polar targets are used to characterize how CPR varies as a function of bistatic angle for craters deposits in which the presence of water ice is not expected (red line in figure 1).

Non-Polar Craters: Non-polar craters for which data has been acquired, to date, include the 4 km diameter crater La Condamine S (57.3°N, 25.2°W) and the 31 km diameter crater Kepler (8.1°N, 38.0°W). These were chosen because of their well-defined ejecta blankets. The Kepler ejecta blanket has been imaged several times and we now have data covering bistatic ranging from 0° to ~20°.

Figure 2 shows an example of a CPR and Bistatic Angle map for a Kepler collect and figure 3 shows some preliminary analyses of how CPR varies with bistatic angle for both impact ejecta, and mare terrain.

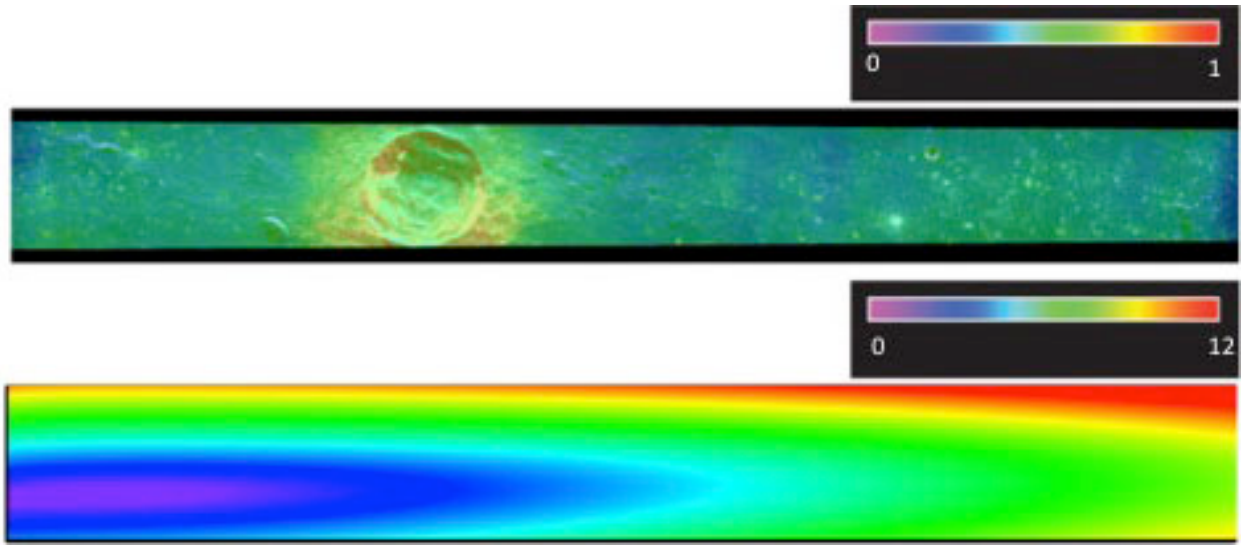

Figure 2. The top image shows a CPR image of Kepler crater acquired by Mini-RF and Arecibo in a bistatic mode. The bottom image shows the range of bistatic (phase) angles associated with the radar data.

Polar Craters: We have made good progress in characterizing the bistatic radar properties of ejecta and mare terrains (figure 3) and are now concentrating activities on polar targets. We have imaged several craters in the south polar region with a special focus on the LCROSS target Cabeus crater [8].

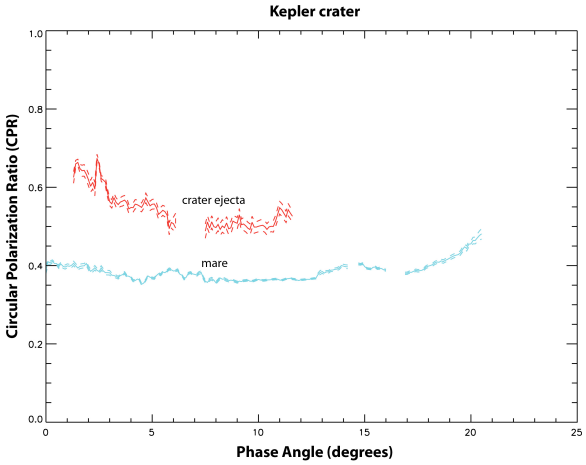

Figure 3: Preliminary analysus showing how CPR varies with bistatic (phase) angle for both ejecta and mare terrain.

Conclusions: Using Arecibo and Mini-RF we are acquiring the first ever planetary bistatic radar images of the lunar surface. These data provide a unique new piece of evidence to determine if the Moon's polar craters contain ice. We are looking to see if monostatic high-CPR polar craters have high or low values in the bistatic data. If we find areas that become low only in the bistatic data then this provides strong supporting evidence that these are ice deposits.

References: [1] Raney, R. K. et al. (2011), *Proc. of the IEEE 99*, 808-823; [2] Campbell B. et al. (2006) *Nature*; [3] Spudis P.D. et al. (2010) *GRL* [4] Spudis et al. (2013), *JGR 118*, 1-14 [5] Carter et al. (2012), *JGR 117*, E00H09; [6] Ghent et al. (2010), *Icarus 209*, 818-835; [7] Goswami and Annadurai (2009), *Current Science 96*, 486; [8] Patterson G. W. et al. (2014) *LPSC XLV*.